THE JOURNAL OF PHYSICAL CHEMISTRY LETTERS
A JOURNAL OF THE AMERICAN CHEMICAL SOCIETY

pubs.acs.org/JPCL

Letter

A Simple Solution to Trivial Crossings: A Stochastic State Tracking Approach

Story Temen and Alexey V. Akimov*

Cite This: J. Phys. Chem. Lett. 2021, 12, 850–860

Read Online

ACCESS | Metrics & More | Article Recommendations | Supporting Information

ABSTRACT: We present a new state tracking algorithm based on a stochastic state reassignment that reflects the quantum mechanical interpretation of the state time-overlaps. We assess the new method with a range of model Hamiltonians and demonstrate that it yields the results generally consistent with the deterministic min-cost algorithm. However, the stochastic state tracking algorithm reduces magnitudes of the state population fluctuations as the quantum system evolves toward its equilibrium. The new algorithm facilitates the thermalization of quantum state populations and suppresses the population revivals and oscillations near the equilibrium in many-state systems. The new stochastic algorithm has a favorable computational scaling, is easy to implement due to its conceptual transparency, and treats various types of state identity changes (trivial or avoided crossings and any intermediate cases) on equal footing.

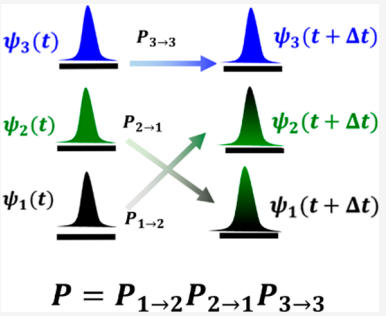

Nonadiabatic molecular dynamics (NA-MD) is a powerful method to study the dynamics of excited states,[1−5] including charge and energy transfer processes in various systems. In particular, quantum-classical trajectory surface hopping (TSH) algorithms, such as the Tully's fewest switches surface hopping (FSSH),[6] are the most widely used techniques due to their conceptual simplicity and computational efficiency that enable a straightforward use of the TSH-like algorithms in modeling of nonadiabatic dynamics (NAD) in complex systems.[7−20] The TSH-based NAD calculations rely on the classical path approximation (CPA),[6,21] according to which nuclei evolve classically, following the Newtonian equations of motion. Each trajectory evolves on a state-specific potential energy surface (PES). At every moment in time, each trajectory can be associated with only a single electronic state, which may change stochastically with the probabilities determined by the evolution of electronic degrees of freedom. Such evolution is dictated by the time-dependent Schrodinger equation (TD-SE):

$$i\hbar\frac{\partial\Psi(r,t)}{\partial t} = H(r;R(t))\Psi(r,t) \quad (1)$$

Here, $\Psi(r,t) = \sum_i c_i(t)\psi_i(r;R(t))$ is the overall wave function of the system, where $\{\psi_i(r;R(t))\}$ are the electronic basis functions of the system, parametrically dependent on the overall geometry of the system, $(R(t))$, $\{c_i(t)\}$ are the amplitudes of the electronic states, and $H(r;R(t))$ is the CPA Hamiltonian. The latter is an operator that depends functionally on time and electronic coordinates (r) but depends only parametrically on nuclear geometries, $R(t)$.

The detailed description of the TSH-based NA-MD procedure has been given many times already,[2,6,20,22,23] so there is no need to dive into these details here. What is important for the current discussion is the fact that the identity (the character) of the electronic basis functions used in eq 1 may change over time, unless they are chosen as diabatic. The adiabatic basis states are, however, more commonly used. The adiabatic states are obtained by solving the time-independent Schrodinger equation (TISE) and are ordered according to their energies, so the energy of a state "1" is not larger than the energy of state "2". However, because these states depend on nuclear geometry, their character may change due to the adiabatic evolution of the system. In other words, at a later integration time step $t + \Delta t$ the state "1" may become more similar to the state "2" at an earlier time step t and vice versa, $\psi_1(t+\Delta t) \approx \psi_2(t)$ and $\psi_2(t+\Delta t) \approx \psi_1(t)$ (Figure 1a). In this situation, known as a trivial crossing, the mapping of the state identities and their physical/chemical properties (e.g., charge localization) to their index becomes time dependent. Such mapping needs to be tracked in time so that the population of each state index can be correctly associated with the physical process of charge transfer. This mapping is applied before the TSH hop probability is computed.

The trivial crossing problem has attracted a lot of attention from various researchers.[24−30] Its occurrence is facilitated by small electronic (diabatic) coupling of the involved diabatic states and by the degeneracies of the energy levels. The latter

Received: November 18, 2020
Accepted: January 6, 2021
Published: January 11, 2021

https://dx.doi.org/10.1021/acs.jpclett.0c03428
J. Phys. Chem. Lett. 2021, 12, 850−860

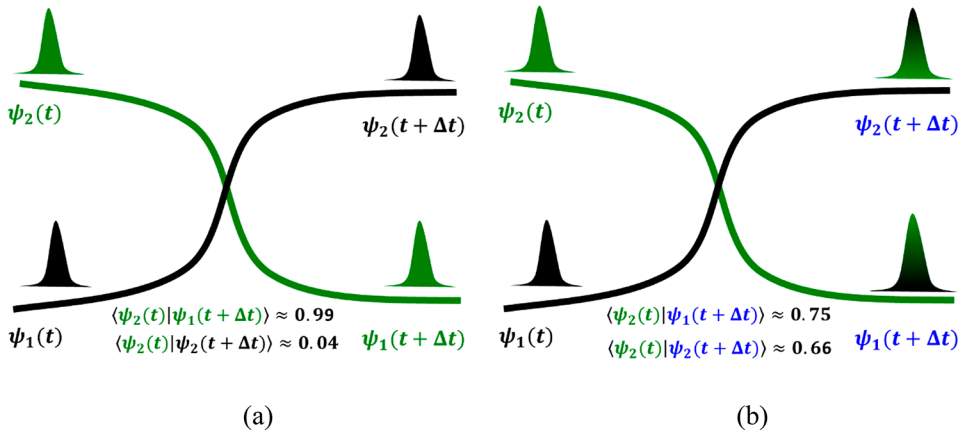

Figure 1. An illustration of two trivial crossing types: (a) a situation when the state tracking is straightforward because the mapping is nearly deterministic; (b) a potentially problematic situation when state assignment may become ambiguous because of notable state mixing during the time step.

scenario is common in complex systems with many states belonging to dense manifolds with rich possibilities for trivial crossings and avoided crossings.[31] In particular, systems like molecular crystals,[32] conjugated aromatic polymers,[33] or chromophore assemblies[34] are remarkable in this regard because having multiple nearly identical molecular sites (molecules or monomers) separated by long distances is the condition that favors the energetic degeneracies and vanishingly small electronic couplings. The trivial crossings are also facilitated by a complex interplay of the multiple inactive "bath" modes and by molecular and nuclear vibration symmetries[35] which all facilitate the adiabatic state crossing in the multidimensional spaces of nuclear coordinates. As an example, an avoided crossing may exist in a 1D problem (one nuclear degree of freedom), but it can be converted to a conical intersection or a more general trivial crossing as the dimensionality of the nuclear degrees of freedom subspace increases. This situation is more typical in photoexcited systems, where conical intersections play the vital role in determining the dynamics of photochemical processes.[36]

Several solutions to identifying trivial crossing have been proposed to date. Fernandez-Alberti et al.[28] relied on the "min-cost" matching algorithm, also known as the Munkres−Kuhn or the "Hungarian" method. In this approach, the states' identity reassignment is made by minimizing the "cost" function. In a nutshell, the overlaps of the adiabatic states at different times are first computed:

$$S_{ij}(t, t+\Delta t) = \langle \psi_i(t) | \psi_j(t+\Delta t) \rangle \tag{2}$$

The state index mapping, $i \rightarrow j$, then corresponds to maximizing time-overlaps, $S_{ij}(t,t+\Delta t)$, provided the mapping is bijective. Ryabinkin el al.[27] suggested a somewhat simplified procedure, where the elements of the time-overlap matrix, $S_{ij}(t,t+\Delta t)$, are first rounded up or down to 0 or ±1, $O(t,t+\Delta t) = round[S(t,t+\Delta t)]$, and the resulting matrix $O(t,t+\Delta t)$ is regarded as the state mapping operator. Recently, Qiu et al.[24] pointed out that the trivial crossings may involve both active states on which the nuclei currently evolve and the nonactive ones at the same time. Accordingly, four scenarios are possible, which can be handled by applying the self-consistent FSSH (SC-FSSH) scheme reported earlier by Wang et al.[26] up to two times to detect possible trivial crossings at the source and target states. The resulting crossingcorrected FSSH (CC-FSSH) methodology[24] provided notable advantages in efficiency and accuracy over the local diabatization and SC-FSSH schemes. Additional computational savings are achieved via adaptive reduction of the size of a subspace of states among which the trivial crossings are possible (narrow energy window).[37] It is worth mentioning that the min-cost approach of Fernandez-Alberti et al.[28] utilizes a state windowing strategy to reject unphysical state reassignments and reduce the costs of calculations by modifying the cost function with an exponential attenuation factor.

Although the mentioned approaches have been demonstrated to be successful in many situations, there are two potential conceptual problems with these approaches. First, the decision of the states' assignment becomes nontrivial when there are more than one comparable matrix elements $S_{ij}(t,t+\Delta t)$ (e.g., consider several different js for a fixed i, Figure 1b). Although the algorithm may eventually pick only one of the many options, there is no solid ground for favoring one of the options to another. Physical intuition tells that if $S_{ij}(t,t+\Delta t) \approx S_{ij'}(t,t+\Delta t), j \neq j'$, that is when there are degenerate or nearly degenerate states involved, the reassignments of the initial state i to either j or j' should occur with comparable frequencies since the original state i is similar to both of the states j and j' to a comparable extent. In this regard, the rounding scheme of Ryabinkin et al.[27] could break the bijective mapping, leading to the ambiguity in state reassignment. For instance, if matrix elements $S_{ij}(t+\Delta t) \approx S_{ij'}(t+\Delta t) > \frac{1}{2}$, their rounding leads to two 1's, so the original state i could be mapped to both states j and j', at which point one would need to use an additional criterion to decide on whether the state i transforms to state j or to state j'. It is desirable that the state tracking algorithm would not break the bijectivity of the state mapping and could account for a situation with multiple comparable time-overlap matrix elements where the states' reassignment may be ambiguous.

The second concern is related to the conceptual/implementation complexity of the existing methods. In particular, the min-cost algorithm requires a lot of bookkeeping and is not straightforward to implement and modify. The algorithm also originates as an abstract optimization problem rather than an approach based on quantum mechanical grounds. As far as the CC-FSSH method is concerned, it involves many conditional operations (e.g., accounting for four

https://dx.doi.org/10.1021/acs.jpclett.0c03428
J. Phys. Chem. Lett. 2021, 12, 850−860

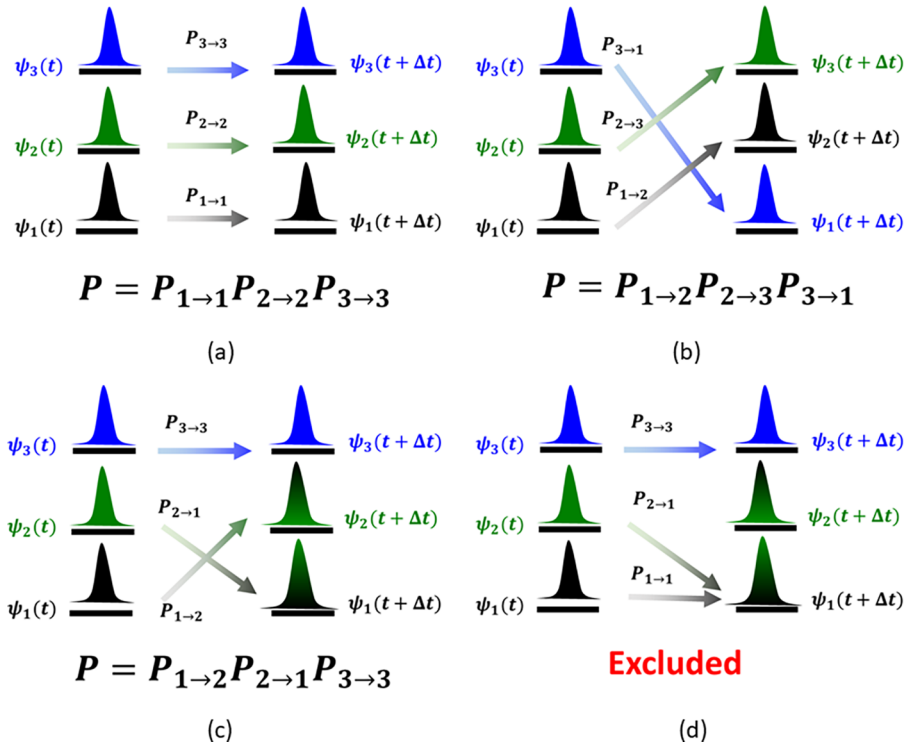

Figure 2. Some possible scenarios of the state identity evolution in a three-level system. The color of the wavepacket represents the character of the state, such that the time-overlaps are larger for the states of the same color. (a) No trivial crossings in all states. (b) All states experience trivial crossing, leading to the states to permute their identities as [1,2,3] → [2,3,1]. (c) A situation when two of the states (ψ_1 and ψ_2) at the time step $t + \Delta t$ have strong mixing of the states $\psi_1(t)$ and $\psi_2(t)$, so that state indices can permute as [1,2,3] → [1,2,3] or [1,2,3] → [2,1,3] with comparable probabilities. (d) The proposed nonbijective permutations are rejected.

types of crossings) and additional procedures that go beyond the standard TSH (e.g., FSSH) prescription and may require substantial efforts in ensuring the correctness of its implementation.

In this work, we introduce a simple algorithm that resolves the potentially ambiguous state assignment problem, is conceptually simple (which translates into its simple implementation that is easy to integrate with standard TSH schemes), and has a favorable computational complexity. The algorithm is designed to address only the state assignment problem and is meant to be used alongside any of the existing TSH algorithms for nonadiabatic dynamics. In particular, in this work we utilize it with Tully's FSSH scheme[6] as implemented in the Libra package.[38]

The key idea of the approach is the interpretation of the time-overlaps, eq 2. Consider re-expanding any current state (at time t), $\psi_i(t)$ in the basis of the time-evolved (at time $t + \Delta t$) states, $\psi_j(t + \Delta t)$:

$$\psi_i(t) = \sum_k a_{k,i}\psi_k(t + \Delta t) \tag{3}$$

Assuming the orthonormality of each set, one finds that

$$a_{j,i} = \langle \psi_j(t + \Delta t)|\psi_i(t)\rangle = S_{ij}(t, t + \Delta t) \tag{4}$$

The measure of a similarity of a state $\psi_i(t)$ to any state $\psi_j(t + \Delta t)$ is then given by the squares of quantum amplitudes, $|a_{j,i}|^2 = |S_{ij}(t,t + \Delta t)|^2 = |S_{ij}(t,t + \Delta t)|^2$. In other words, the probability for a state $\psi_i(t)$ to become a state $\psi_j(t + \Delta t)$ adiabatically (state identity change) is

$$P_{i\to j} = \frac{|S_{ij}(t, t + \Delta t)|^2}{\sum_k |S_{ik}(t, t + \Delta t)|^2} \tag{5}$$

Equation 5 is the key of the proposed algorithm. Instead of the deterministic state reassignment utilized by other algorithms, we use a stochastic reassignment. That is, state identities can be reassigned to any other one at every step with the probabilities proportional to the squared magnitudes of the corresponding time-overlaps. Importantly, in our approach, the reassignment process involves not only the active states but also all initial and all final states. This means that for any state to change its index, there should be no conflicting identity changes associated with other states. The states' reassignment based on eq 5 reflects the adiabatic mechanism of quantum state transfer (switching from one state to another due to change of the states' identities). As mentioned above, eq 5 is to be used in combination with standard TSH schemes of the user's choice (e.g., FSSH) which would account for nonadiabatic mechanisms of quantum state transfer (switching due to nonadiabatic coupling).

Based on eq 5 for probabilities of the adiabatic state transitions $i \to j$, we compute the probabilities for the collective transitions of all states:

$$P_{I\to J} = \frac{1}{|P|}\prod_{i\in I, j\in J} P_{i\to j} \tag{6}$$

Here, $I = (i_1, i_2, \cdots, i_N)$ and $J = (j_1, j_2, \cdots, j_N)$ are the multistate indices that reflect the ordering (permutations) of all adiabatic states before and after a proposed state identity change, N is the number of states, and $|P| = \sum_{I,J}\prod_{i\in I, j\in J} P_{i\to j}$ is the

https://dx.doi.org/10.1021/acs.jpclett.0c03428
J. Phys. Chem. Lett. 2021, 12, 850−860

normalization factor (with the double sum effectively running over all possible permutations). The products of eq 6 are used to determine the states' reassignments. Because at this level we use the collective indices (possible permutations), the decision on state identity reassignment is made collectively and reflects the potential changes of the identities of all states, not just a single one (e.g., the active state). For instance, for a 3-state system (e.g., Figure 2) the product of the type $P = P_{1\to1}P_{2\to2}P_{3\to3}$ would be proportional (up to the normalization factor $|P|$) to the probability for all three states to keep their identities unchanged (no state reassignments). As we mentioned above, the regular TSH hopping schemes (including frustrated hops) are still applied alongside the state tracking algorithm. Stated differently, the algorithm computes the probabilities of each possible state identity permutation, using eqs 5 and 6, and it accepts one of the such permutations with the corresponding probabilities.

We illustrate the idea of the algorithm by considering possible state reordering situations in a 3-state system (Figure 2). In a first scenario, none of the states experience significant character change, and all probabilities for each state to keep its original index are close to one, $P_{i\to i} \approx 1$ (Figure 2a). In this situation, the probability for the overall state index permutation to stay an identity permutation, $[1,2,3] \to [1,2,3]$, is also close to one, $P = P_{1\to1}P_{2\to2}P_{3\to3} \approx 1$. In a second scenario, one may encounter one or more clear trivial crossings at the same time (Figure 2, panels b and c). The clarity in this context means that the probabilities of the corresponding transformations are close to one, $P_{i\to j} \approx 1$, $i \neq j$. This scenario is the most suitable for the deterministic approaches mentioned. The deterministic algorithms are therefore expected to handle these situations well. As before, the probability of the overall permutations (e.g., $[1,2,3] \to [2,3,1]$ as shown in Figure 2a) is close to 1, but only approximately; there is still a possibility for less likely state index permutations to occur which can be regarded as a manifestation of electronic tunneling. We emphasize that the algorithm does not introduce nuclear tunneling since the nuclei are still treated fully classically using trajectory surface hopping. Finally, in a third scenario one may encounter multiple permutations that can occur with notable probabilities. For instance, one may have the original states $\psi_1(t)$ and $\psi_2(t)$ strongly mix within the integration time step interval, $[t,t + \Delta t]$, making the new states $\psi_1(t + \Delta t)$ and $\psi_2(t + \Delta t)$ resemble each of the two starting states. In this case, the probabilities of the state changes $\psi_1(t) \to \psi_1(t + \Delta t)$ and $\psi_1(t) \to \psi_2(t + \Delta t)$ as well $\psi_2(t) \to \psi_1(t + \Delta t)$ and $\psi_2(t) \to \psi_2(t + \Delta t)$ may all be comparable to each other. As a result, the state index permutations $[1,2,3] \to [1,2,3]$ and $[1,2,3] \to [2,1,3]$ should be possible and occur with comparable probabilities. This is the situation the present stochastic state tracking algorithm is designed to handle, since it would simply consider each of the possible permutations with the corresponding overall probabilities. On the contrary, the deterministic algorithms would always pick only one of the permutations.

As far as the implementation of the algorithm goes, there is an important aspect that we comment on. There are several ways the algorithm can be implemented. One approach would be to consider a sequential assignment of each state index followed by the renormalization of state index reassignment probabilities, $P_{i\to j}$. However, such an approach would yield different results depending on the order in which the states are excluded. Our early experimentations with such an approach showed that it may lead to incorrect state population dynamics. Thus, it is important to handle the reassignments of all states collectively, as also described above. In this approach, one can construct all possible state permutations and compute the probabilities of each of them to occur. By selecting the permutation with the corresponding probabilities, one selects a unique state identity reassignment every time. The apparent drawback of this approach is the scaling of its computational costs. Since the number of possible permutations of N states grows as $N!$, such a scheme is unpractical for all but systems with a very small number of states (e.g., $N < 5$). Thus, our ultimate implementation of the stochastic assignment procedure is as follows. For each initial state i, $i = 1, \cdots N$, we propose a change to a state j with the probability $P_{i\to j}$. We then verify if the overall reassignment is bijective; that is, there are no reassignments of different initial states to the same final state index (Figure 2d). If the overall permutation is bijective, it is accepted and the all state indices are reassigned according to such proposed permutation. If the permutation is problematic, it is rejected and the procedure is repeated until an acceptable permutation is found. Provided enough attempts, a proper permutation can always be found. In practice, the likelihood of such an event depends on the probabilities for multiple states to "become" a common one. Under such conditions, the number of unsuccessful (and eventually rejected) attempts may be quite large, which may be a potential limitation of this approach. We shall also comment that the proposed state identity "transitions" in Figure 2d are not to be confused with the "frustrated" hops done as the part of the regular TSH algorithms for nonadiabatic transitions. The latter are needed to impose the physically meaningful energy partitioning between electrons and nuclei, whereas the former is simply a way to ensure that the stochastic adiabatic "transitions" respect the bijectivity.

By construction, the stochastic state tracking algorithm addresses the requirements we discussed above. First, it naturally resolves possibly ambiguous state assignments (e.g., see Figure 1b). Considering that one has to run a sufficiently large number of trajectories to obtain reliable statistics, the stochastic nature of assignment is not a problem. Quite on the contrary, it is more consistent with the quantum mechanical interpretation of the time-overlaps and may have a potential to account for some amount of quantum mechanical (electronic) tunneling, as alluded to above. If a state at time t is similar to more than one state at time $t+\Delta t$, one should be able to account for possible quantum mechanical branching (of adiabatic transitions). The definition of state change probabilities, eq 5, also implies that if a state does not really change adiabatically ($S_{ii}(t,t + \Delta t) = 1, S_{ij}(t,t + \Delta t) = 0, \forall j \neq i$), the assignment procedure will ensure the state's identity does not change (i stays i), as one would expect in the adiabatic limit. In the case the matrix elements are reasonably close to unity, the state's identity would stay unchanged with a high (nearly 100%) probability. A similar situation is the case of avoided crossings. In fact, the avoided crossing with the large adiabatic gap (strong electronic coupling) is the adiabatic limit. As the electronic coupling of the diabatic states decreases, one may still be in the regime of avoided crossings but with larger nonadiabatic couplings. In this situation, the application of eq 5 provides a natural treatment of state tracking, intermediate between the fully adiabatic dynamics (where no state changes occur) and the trivial crossings (where the state changes occur with nearly 100% probability). Thus, eq 5 provides a simple

https://dx.doi.org/10.1021/acs.jpclett.0c03428
J. Phys. Chem. Lett. 2021, 12, 850−860

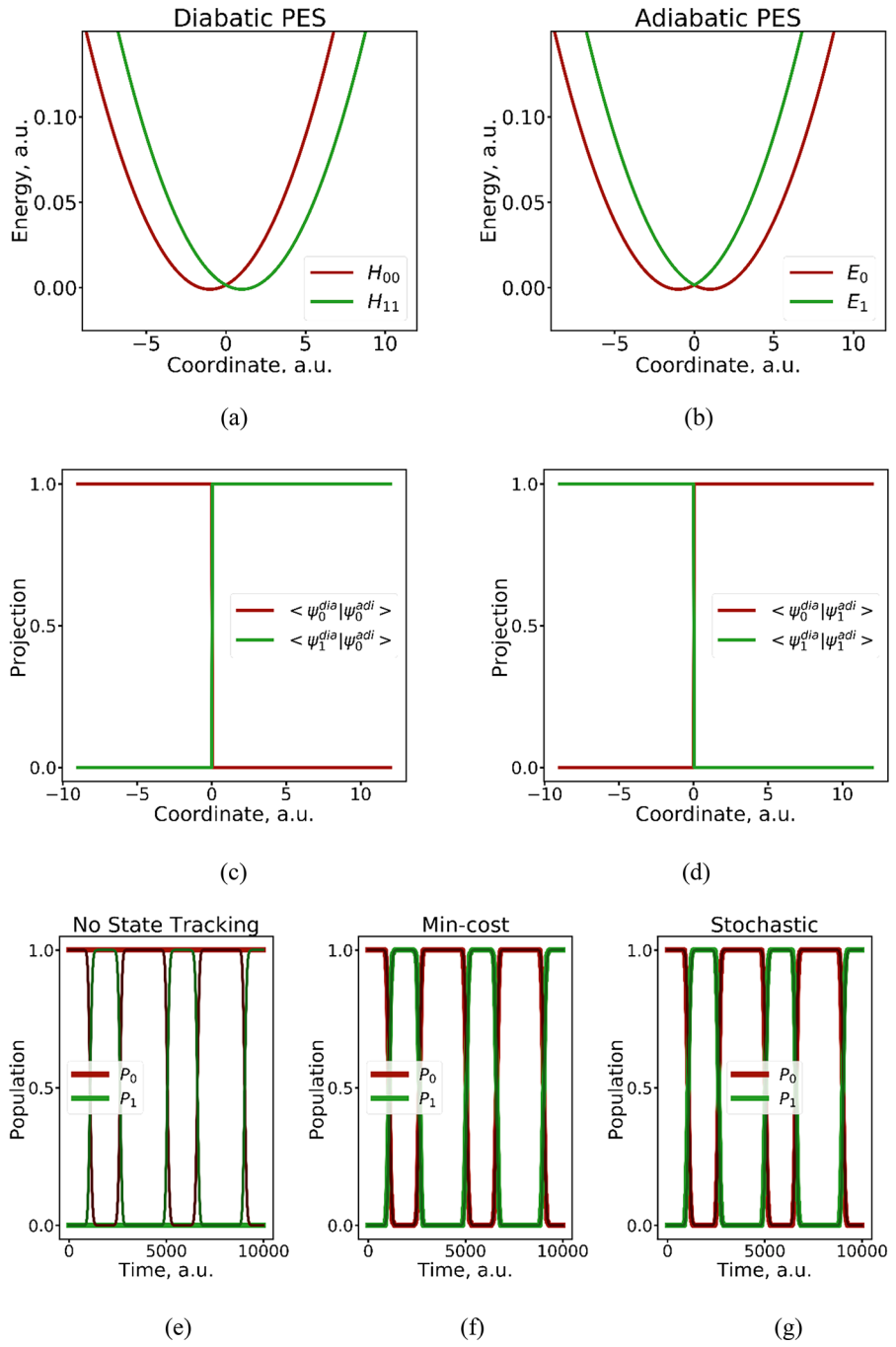

Figure 3. A simple 2-state model: (a) diabatic and (b) adiabatic state energies as the functions of the nuclear coordinate. Projections of the first (c) and second (d) adiabatic states on the diabatic states as the function of nuclear coordinate. Populations of all adiabatic states as a function of time as computed using FSSH with one of the state tracking options: (e) no state tracking, (f) min-cost tracking, and (g) stochastic tracking algorithm. Thick lines correspond to the FSSH results, and the thin lines correspond to the SOFT dynamics.

and general way of handling three types of state identity change scenarios on equal footing.

Second, the algorithm accounts for possible changes of states' identities for all states, not just the active one. In this regard, it naturally covers the four types of situations the crossing corrected state tracking algorithm is designed to handle. In doing so, the stochastic tracking algorithm does not require a complex set of conditional (often nested) statements and keeps conceptual and implementation simplicity. Third, the definition of the algorithm (e.g., Figure 2) ensures that the state reordering always stays bijective and there are no situations when two current states $\psi_i(t)$ and $\psi_{i'}(t)$ both map into the same new state $\psi_j(t + \Delta t)$.

To demonstrate the utility of the devised stochastic state tracking algorithm, we consider several model problems of a spin-boson type that correspond to various regimes that may be encountered in complex systems with multiple electronic states. The detailed description of the parameters for each model is given in the Supporting Information, Section 1. In the diabatic representation, the Hamiltonian matrix elements are represented as displaced harmonic oscillators, all coupled to the same single nuclear degree of freedom, x:

https://dx.doi.org/10.1021/acs.jpclett.0c03428
J. Phys. Chem. Lett. 2021, 12, 850−860

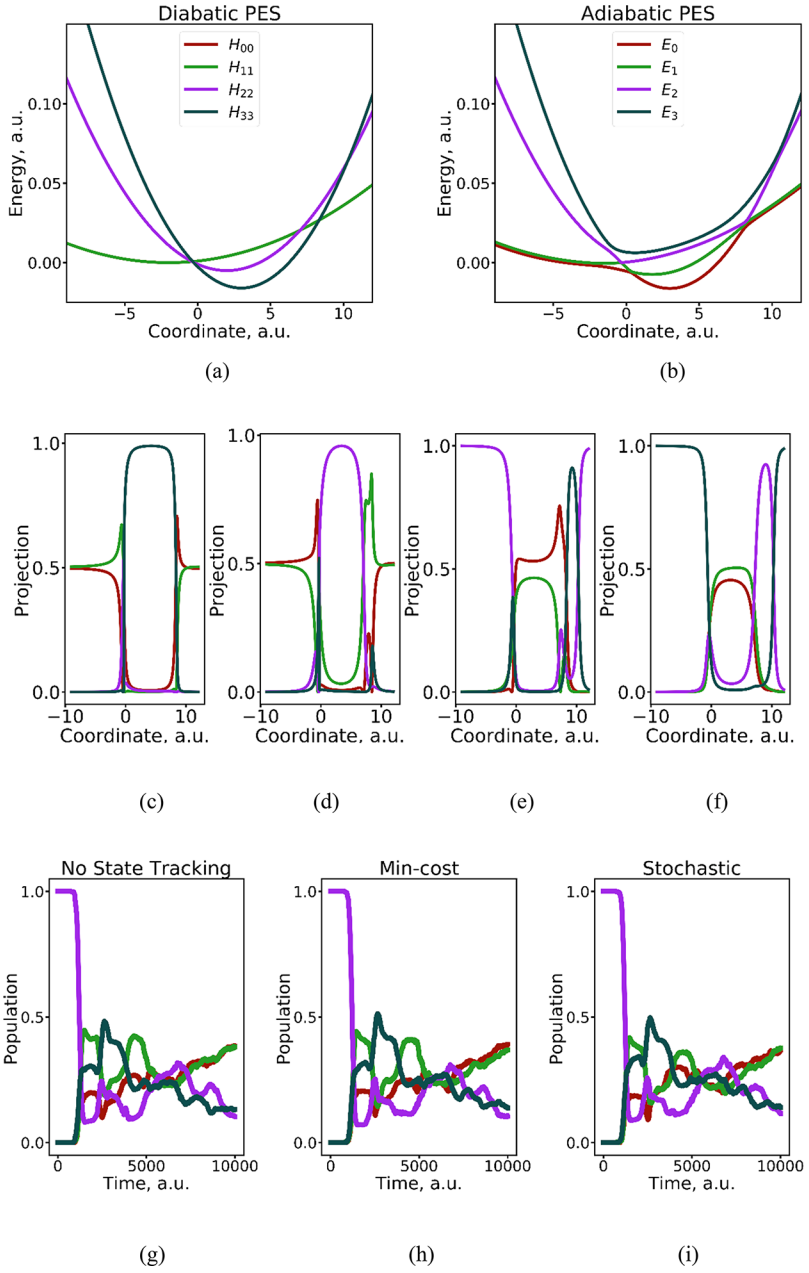

Figure 4. A four-state model with degenerate states and variable couplings: (a) diabatic and (b) adiabatic state energies as the functions of the nuclear coordinate. Projections of the adiabatic states on each of the diabatic states as the function of nuclear coordinate (c–f). Populations of all adiabatic states as a function of time as computed using FSSH with one of the state tracking options: (g) no state tracking, (h) min-cost tracking, and (i) stochastic tracking algorithm.

$$H_{ii} = E_i + \frac{1}{2}k_i(x - x_i)^2 \tag{7a}$$

$$H_{ij} = V_{ij} = const,\ i \neq j \tag{7b}$$

The off-diagonal elements of the electronic Hamiltonian, eq 7b, are taken to be constant and are varied to control the topology of adiabatic state intersections/crossing as well as the degree of mixing of diabatic states in adiabatic ones. Such spin-boson type models are suitable to mimic typical energy levels' dynamics and multiple state crossings, often observed in complex (e.g., solid-state or nanoscale) systems.

Since this work focuses on the identification and handling of trivial (and less trivial) crossings, we conduct all the TSH calculations using the FSSH algorithm implementation in the Libra package.[38] Note that the current calculations utilize the original FSSH scheme, including explicit treatment of electron–nuclear back-reaction. The dynamics parameters are provided in the Supporting Information, Section 2. For all considered models, the dynamics is computed using different state tracking options, i.e., no state tracking, min-cost, and the current stochastic. In addition, a numerically exact integration of the TD-SE on a 1D grid is conducted using the split operator Fourier transform (SOFT) method of Kosloff and Kosloff,[39] also available in Libra. The numerically exact dynamics is computed only to provide a general guidance on how the accurate state population dynamics shall look like. We do not aim to assess the role of the state tracking algorithm in providing accurate population dynamics, since FSSH does not

https://dx.doi.org/10.1021/acs.jpclett.0c03428
J. Phys. Chem. Lett. 2021, 12, 850–860

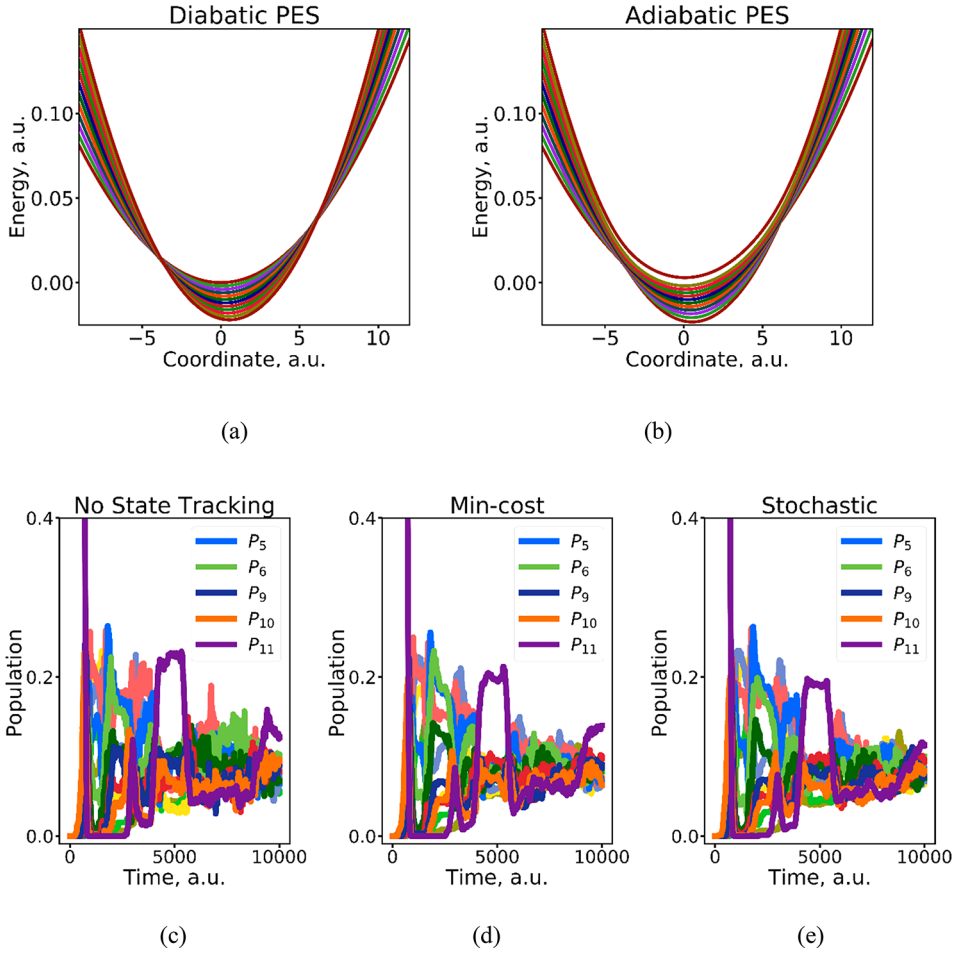

Figure 5. A 12-state model with variable electronic couplings: (a) diabatic and (b) adiabatic state energies as the functions of the nuclear coordinate. Populations of all adiabatic states as a function of time as computed using FSSH with one of the state tracking options: (c) no state tracking, (d) min-cost tracking, and (e) stochastic tracking algorithm.

account for other quantum effects such as quantization of nuclear DOFs and electronic decoherence. Comparing and discussing accuracies would require using more sophisticated methods than FSSH which might be a totally separate study and goes beyond the scope of this work. For this reason, we primarily assess the quality of the new method by comparing its performance with that of the well-established but conceptually different min-cost algorithm. Therefore, the results of the SOFT dynamics for models II and III are only available in the Supporting Information, Section 3.

The nuclear subsystem is represented by a single degree of freedom with an effective mass of m = 2,000 a.u. In all TSH calculations, 2000 trajectories are utilized, although the results converge already with 500 trajectories. The initial coordinates and momenta of all particles (trajectories) are sampled from the normal distributions with the mean values of both coordinates and momenta specified below. The variances of these properties are given by $\sigma_x^2 = \frac{1}{2a}$ and $\sigma_p^2 = \frac{a\hbar^2}{2}$, where $a = \frac{m\omega}{\hbar}$ and $\omega = \sqrt{\frac{k}{m}}$. Here, $k = 0.005\frac{\text{Ha}}{\text{Bohr}^2}$ is chosen as the curvature of the diabatic surfaces that define the probability distributions. Note although we generally choose this parameter to be consistent with the force constants that appear in eqs 7a and 7b, they may be chosen freely. Such a scheme corresponds to sampling from the ground state of the 0th diabatic potential energy surface (centered on x = 0). The chosen model and particle parameters yield the characteristic frequency of $\omega \approx 0.158$ a.u., which is 2121 cm^{-1}, a typical value for many condensed-matter environments. The coupled electron−nuclear dynamics for all models is integrated for 10000 steps with the integration time step of 1 a.u., thus corresponding to approximately 250 fs trajectories. The convergence with respect to the number of trajectories and size of the time step is confirmed for all models (Section 4 of the Supporting Information). We find that the number of trajectories and the integration time step required to achieve the converged results are generally comparable for any state tracking option.

Model I. The first model is represented by two noninteracting ($V_{01} = V_{10} = 0$) diabatic surfaces (Figure 3a), leading to the conical intersection in the adiabatic representation (Figure 3b). The trajectories are initialized on the ground adiabatic state (index 0) with the mean of the probability density distribution being −4.0 a.u. for coordinate and 2.0 a.u. for momentum. As the projection in Figure 3c demonstrates, the adiabatic state 0 in this region is completely composed of the diabatic state 0. Because the diabatic surfaces are uncoupled, the dynamics can be understood as the evolution of the trajectories on the red diabatic parabola. Because of the initial conditions, the trajectories have enough kinetic energy to pass the region of surface crossing (x = 0) after which the diabatic state 0

https://dx.doi.org/10.1021/acs.jpclett.0c03428
J. Phys. Chem. Lett. 2021, 12, 850−860

coincides with the adiabatic state 1, which is also seen in the projection in Figure 3d. Thus, the dynamics shall consist of periodic transfer of the entire population between the adiabatic states 0 and 1. This dynamics is indeed observed with numerically exact integration of the TD-SE (Figure 3, panels e−g, thin lines) as well as in FSSH calculations with state tracking done by the min-cost (Figure 3f, thick lines) and stochastic (Figure 3g, thick lines) algorithms. Because the coupling between diabatic states is constant, and its derivative with respect to the nuclear coordinate is zero, the nonadiabatic coupling between the adiabatic states is also zero. Thus, once started on the adiabatic surface 0 and not accounting for state tracking, one predicts no population transfer from the initial adiabatic state (Figure 3e, thick lines).

Model II. Next, we consider a four-state model, in which the diabatic states 0 and 1 are degenerate, $H_{00} = H_{11}$, and all the states are weakly coupled to each other, $V_{03} = V_{30} = V_{12} = V_{21} =$ 0.002 Ha and $V_{ij} = 0.002$ Ha $\forall\ i, j, i \neq j$ for all other pairs of states. All four states also cross in one point (in a diabatic representation), as illustrated in Figure 4a. As a result, the topology of the adiabatic energy surfaces features the trivial crossings, multiple avoided crossings, and the regions of near degeneracy of adiabatic states (Figure 4b). Remarkably, the point at $x \approx 8$ features an avoided crossing between state 2 (purple) and two states (0 and 1) that become nearly degenerate past this point ($x > 8$) but are well separated in the range $0 < x < 8$. As the analysis of the adiabatic-to-diabatic state projections (Figure 4, panels c−f) shows, in the regions $x < 0$ and $x > 10$, the composition of the adiabatic states 0 and 1 are similar in the regard that they both mix about 50% of diabatic states 0 and 1 each. A similar situation occurs for the adiabatic states 2 and 3 in the region $0< x < 10$. Thus, one may expect the adiabatic transitions $\psi_0(t) \rightarrow \psi_0(t + \Delta t)$ and $\psi_0(t) \rightarrow \psi_1(t + \Delta t)$ to be potentially competitive with each other in the first range and the transitions $\psi_2(t) \rightarrow \psi_2(t + \Delta t)$ and $\psi_2(t) \rightarrow \psi_3(t + \Delta t)$ to be competitive in another range.

In our calculations, the trajectories are initialized on adiabatic state 2. Their initial coordinates are sampled from a normal distribution centered around $x = -5$ a.u. with zero mean momentum. With such starting conditions, all trajectories have enough energy to explore all the regions of the designed model and hence experience all the types of topologies. The computed evolution of the populations (Figure 4, panels g−i) can be understood in the following way. The initial population of the state 2 depletes rapidly once the trajectories travel down to the region of multiple crossings at $x \approx 0$. Here, the population is split into 10−40% and deposited in each of the four states. As the slope of the adiabatic surface E_2 suggests, the state converts to adiabatic state 1 (green) and then 0 (red) as one passes $x = 0$ in the positive direction. Such transitions need to be tracked. Without the tracking (Figure 4g), only a small population of ca. 0.1 is transferred to state 1. When the tracking is enabled, one determines to stay on the current state (which is now relabeled as 1) with a higher probability, so about 0.4 population is accumulated on it. Accumulation of the population on state 0 follows the decay of transient population of state 1, if the states are tracked. If they are not tracked, the state 0 is populated in parallel with the decay of the state 2. Importantly, the population dynamics computed with both min-cost and stochastic state tracking algorithms are nearly identical. The minor differences are negligible in comparison to the dynamics when population is not tracked.

Model III. Finally, we consider a 12-state model with a dense manifold of electronic states (Figure 5, panels a and b). The PES are nearly parallel to each other, so the energy gap fluctuations are expected to be rather small. This model is designed to mimic a typical situation one encounters in modeling of excited states dynamics in condensed matter systems. However, unlike in most condensed-matter systems, the diabatic energy levels are made to cross with many other such surfaces in two areas. In such points ($x \approx -4$ and $x \approx 6$), all adiabatic surfaces are coupled to adjacent states and to states that are two indices away (i.e., state 1 is coupled to states 2 and 3). As a result, one may end up with the time-overlaps for many pairs of states being comparable, hence favoring the accumulation of the overall difference in the dynamics with states tracked with min-cost or stochastic algorithms.

For this model, the trajectories are initialized in the highest excited state. Their initial coordinates are sampled from a normal distribution centered around $x = -8$ a.u., which corresponds to a high-energy region. The initial momentum is zero on average, but the slope of the adiabatic surface creates the force sufficient to quickly drive the trajectories in the region of their strong coupling. As in the previous example, the trajectories have enough energy to explore various topologies of the adiabatic PES manifold encountered in this model.

In NAD calculations with this model, we observe a rapid depopulation of the initial state (Figure 5, panels c−e, purple line) concerted with the populations transfer into several other states. This rapid depopulation of the initial state is followed by the coherent population transfer between several states. The oscillatory features level out at longer time scales, equilibrating the populations of multiple states. Interestingly, despite the construction of the model to favor similarities among multiple states (comparable time-overlaps), the state tracking does not make much difference in the computed dynamics. This may be attributed to the rapid population transfer between states that leads to quick thermalization of their populations. In this scenario, it becomes less critical to know the details of the mechanism by which the equilibrium populations are achieved. Despite the overall similarity of the dynamics computed without state tracking or with any of them, there is a slight difference in the dynamics computed with the min-cost (Figure 5d) and stochastic state tracking (Figure 5e) algorithms. Namely, the stochastic algorithm leads to somewhat smaller fluctuations of populations of all states once they reach the near-equilibrium values. This effect may reflect the small probability of the adiabatic population transfer between states captured by the algorithm.

Finally, we compare the computational scaling of the min-cost and stochastic algorithms (Figure 6) using model time-overlap matrices that mimic various types of state identity changes over time (please see Supporting Information, Section 5). We consider four types of time-overlap matrices. The matrices of the first kind have their main diagonal elements being close to 1.0, with all other elements set to random small values (Figure 6, non-deformed). Such matrix type corresponds to a situation when the state identities do not change, and no state tracking is needed. The other three kinds of matrices are generated by deforming the well-behaved matrix of the first kind. One way the matrix is deformed is by randomly swapping columns (Figure 6, crossings). This deformation type mimics trivial crossings. Another type of matrix deformation simulates the degeneracy of the states during adiabatic dynamics (Figure 6, degeneracy). In this case,

https://dx.doi.org/10.1021/acs.jpclett.0c03428
J. Phys. Chem. Lett. 2021, 12, 850−860

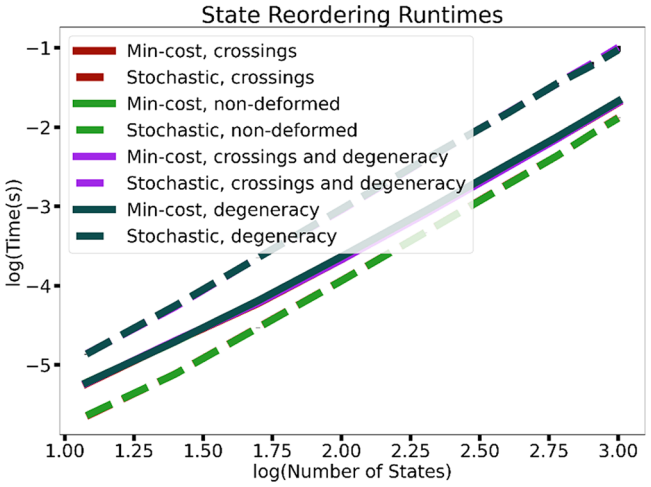

Figure 6. CPU time of the min-cost and stochastic state tracking algorithms as the function of the time-overlap matrix size. The CPU used is an Intel Xeon CPU E5-2620 v3 @ 2.40 GHz. Shown are the timings for several types of time-overlap matrices. Results for several types of calculations are nearly identical, and the corresponding timings are hidden by the solid blue-gray line.

the large time-overlap element on the diagonal is split in half and moved unequally to the two closest states. The original population of these two states is then redeposited into the diagonal matrix element. The last type of matrix deformation combines the previous two to account for simultaneous trivial crossings and state degeneracies (Figure 6, crossings and degeneracy).

The timing of the min-cost algorithm does not depend on the type of the matrix, only on the size of the matrix. This robustness of the min-cost algorithm originates from its deterministic nature. The optimization algorithm works the same way no matter the values of the matrix elements. In contrast, the run time of the stochastic algorithm depends on the structure of the time-overlap matrix. For the non-deformed matrices, we observe shorter run times in comparison to the min-cost. This is because for such matrices the correct state assignment (identity) is found in one attempt, yet without the additional machinery of the min-cost algorithm. As a result, the computing prefactor goes down, although the scaling does not change. Similarly, the stochastic algorithm has a shorter run time for the matrices with crossings and no degeneracy. Here, the correct permutation is also found in one attempt, although it is not the identity permutation. On the other side of the complexity spectrum is when multiple states at time $t-\Delta t$ have a large overlap with the same state at time t (several elements of a given column are comparable). In this situation, the stochastic algorithm will be often proposing the state reassignments of the type shown in Figure 2d that cannot be accepted. The probability of an acceptable state reassignment is small in this case, leading to larger number of attempted "hops". Under certain, particularly unfavorable conditions, the acceptable reassignment may not be found within the predefined limiting number of attempted hops, leading to difficulties in convergence of the stochastic state tracking procedure. Having mentioned that, we also comment that in many practice calculations with atomistic systems, the time-overlap matrices have the "non-deformed" or "crossing" structure, in which cases the stochastic algorithm shall not have convergence problems.

Although the apparent robustness of the min-cost algorithm over the new stochastic scheme has a clear practical convenience, it may hide the underlying problems in the state identity assignment. The difficulties in converging the state assignment via the stochastic algorithm may indicate the presence of the state degeneracies that should be treated adequately. We remind that given sufficient number of attempts, a suitable state assignment can be found with the stochastic algorithm, although at an expense of the increased computational cost. At the same time, although the min-cost would find the state reassignment much faster, it may be systematically selecting one of several possible variants, thus artificially biasing the dynamics.

In this work, we report the development and assessment of a new state tracking algorithm based on stochastic state reassignment that reflects the quantum−mechanical interpretation of the state time-overlaps. We demonstrate that the new algorithm is generally consistent with the deterministic min-cost algorithm but is based on a conceptually different viewpoint. The stochastic state tracking algorithm reduces the magnitude of the population fluctuations as the quantum system evolves toward its equilibrium. This effect acts as a thermalization mechanism suppressing the population revivals and oscillations near equilibrium. The new stochastic algorithm is easy to implement due to its conceptual transparency, although may be more time-consuming than the min-cost when multiple state degeneracies may arise and vanish during the dynamics. By its construction, the algorithm handles all types of state identity changes (trivial and avoided crossings and anything in between) on the same conceptual footing. We also hypothesize that the developed stochastic tracking approach may be able to introduce some degree of electronic tunneling in superexchange-like models.[40,41] Studying this question will require a careful design of a suitable model, which may be a subject of future studies. To this end, the results of the FSSH calculations with the stochastic and min-cost algorithms are very similar for a variety of models tested in addition to those discussed in this account. The data presented here are generated with the FSSH and state tracking methods implemented in the Libra package,[38] ver. 4.9.1,[42] available via GitHub.

■ ASSOCIATED CONTENT

Supporting Information

The Supporting Information is available free of charge at https://pubs.acs.org/doi/10.1021/acs.jpclett.0c03428.

Details of the model Hamiltonian and simulation parameters for all models, SOFT dynamics for models II and III, convergences studies, and the description of the model time-overlap matrices for timing calculations (PDF)

■ AUTHOR INFORMATION

Corresponding Author

Alexey V. Akimov − *Department of Chemistry, University at Buffalo, The State University of New York, Buffalo, New York 14260, United States;* orcid.org/0000-0002-7815-3731; Email: alexeyak@buffalo.edu

https://dx.doi.org/10.1021/acs.jpclett.0c03428
J. Phys. Chem. Lett. 2021, 12, 850−860

Author

Story Temen − *Department of Chemistry, University at Buffalo, The State University of New York, Buffalo, New York 14260, United States*

Complete contact information is available at: https://pubs.acs.org/10.1021/acs.jpclett.0c03428

Notes

The authors declare no competing financial interest.

■ ACKNOWLEDGMENTS

The authors acknowledge the computational support of the Center for Computational Research at the University at Buffalo. A.V.A. acknowledges the financial support of the U.S. National Science Foundation, grant no. OAC-NSF-1931366.

■ REFERENCES

(1) Curchod, B. F. E.; Martínez, T. J. Ab Initio Nonadiabatic Quantum Molecular Dynamics. *Chem. Rev.* **2018**, *118*, 3305−3336.
(2) Crespo-Otero, R.; Barbatti, M. Recent Advances and Perspectives on Nonadiabatic Mixed Quantum−Classical Dynamics. *Chem. Rev.* **2018**, *118*, 7026−7068.
(3) Barbatti, M.; Crespo-Otero, R. Surface Hopping Dynamics with DFT Excited States. *Top. Curr. Chem.* **2014**, *368*, 415−444.
(4) Wang, L.; Akimov, A.; Prezhdo, O. V. Recent Progress in Surface Hopping: 2011−2015. *J. Phys. Chem. Lett.* **2016**, *7*, 2100−2112.
(5) Smith, B.; Akimov, A. V. Modeling Nonadiabatic Dynamics in Condensed Matter Materials: Some Recent Advances and Applications. *J. Phys.: Condens. Matter* **2020**, *32*, 073001.
(6) Tully, J. C. Molecular Dynamics with Electronic Transitions. *J. Chem. Phys.* **1990**, *93*, 1061−1071.
(7) Smith, B.; Akimov, A. V. Hot Electron Cooling in Silicon Nanoclusters via Landau−Zener Nonadiabatic Molecular Dynamics: Size Dependence and Role of Surface Termination. *J. Phys. Chem. Lett.* **2020**, *11*, 1456−1465.
(8) Guo, H.; Chu, W.; Zheng, Q.; Zhao, J. Tuning the Carrier Lifetime in Black Phosphorene through Family Atom Doping. *J. Phys. Chem. Lett.* **2020**, *11*, 4662−4667.
(9) Wang, S.; Fang, W.-H.; Long, R. Hydrogen Passivated Silicon Grain Boundaries Greatly Reduce Charge Recombination for Improved Silicon/Perovskite Tandem Solar Cell Performance: Time Domain Ab Initio Analysis. *J. Phys. Chem. Lett.* **2019**, *10*, 2445−2452.
(10) He, J.; Vasenko, A. S.; Long, R.; Prezhdo, O. V. Halide Composition Controls Electron−Hole Recombination in Cesium−Lead Halide Perovskite Quantum Dots: A Time Domain Ab Initio Study. *J. Phys. Chem. Lett.* **2018**, *9*, 1872−1879.
(11) Lystrom, L.; Tamukong, P.; Mihaylov, D.; Kilina, S. Phonon-Driven Energy Relaxation in PbS/CdS and PbSe/CdSe Core/Shell Quantum Dots. *J. Phys. Chem. Lett.* **2020**, *11*, 4269−4278.
(12) Brennan, M. C.; Forde, A.; Zhukovskyi, M.; Baublis, A. J.; Morozov, Y. V.; Zhang, S.; Zhang, Z.; Kilin, D. S.; Kuno, M. Universal Size-Dependent Stokes Shifts in Lead Halide Perovskite Nanocrystals. *J. Phys. Chem. Lett.* **2020**, *11*, 4937−4944.
(13) Wang, H. I.; Infante, I.; Brinck, S. t.; Canovas, E.; Bonn, M. Efficient Hot Electron Transfer in Quantum Dot-Sensitized Mesoporous Oxides at Room Temperature. *Nano Lett.* **2018**, *18*, 5111−5115.
(14) Akimov, A. V. Nonadiabatic Molecular Dynamics with Tight-Binding Fragment Molecular Orbitals. *J. Chem. Theory Comput.* **2016**, *12*, 5719−5736.
(15) Rego, L. G. C.; Bortolini, G. Modulating the Photoisomerization Mechanism of Semiconductor-Bound Azobenzene-Functionalized Compounds. *J. Phys. Chem. C* **2019**, *123*, 5692−5698.
(16) Yazdani, N.; Bozyigit, D.; Vuttivorakulchai, K.; Luisier, M.; Infante, I.; Wood, V. Tuning Electron−Phonon Interactions in Nanocrystals through Surface Termination. *Nano Lett.* **2018**, *18*, 2233−2242.
(17) Rego, L. G. C.; Hames, B. C.; Mazon, K. T.; Joswig, J.-O. Intramolecular Polarization Induces Electron−Hole Charge Separation in Light-Harvesting Molecular Triads. *J. Phys. Chem. C* **2014**, *118*, 126−134.
(18) Pal, S.; Trivedi, D. J.; Akimov, A. V.; Aradi, B.; Frauenheim, T.; Prezhdo, O. V. Nonadiabatic Molecular Dynamics for Thousand Atom Systems: A Tight-Binding Approach toward PYXAID. *J. Chem. Theory Comput.* **2016**, *12*, 1436−1448.
(19) Zheng, Q.; Chu, W.; Zhao, C.; Zhang, L.; Guo, H.; Wang, Y.; Jiang, X.; Zhao, J. Ab Initio Nonadiabatic Molecular Dynamics Investigations on the Excited Carriers in Condensed Matter Systems. *Wiley Interdiscip. Rev.: Comput. Mol. Sci.* **2019**, *9*, No. e1411.
(20) Akimov, A. V.; Prezhdo, O. V. The PYXAID Program for Non-Adiabatic Molecular Dynamics in Condensed Matter Systems. *J. Chem. Theory Comput.* **2013**, *9*, 4959−4972.
(21) Nikitin, E. E. *Theory of Elementary Atomic and Molecular Processes in Gases*; Clarendon: Oxford, 1974.
(22) Drukker, K. Basics of Surface Hopping in Mixed Quantum/Classical Simulations. *J. Comput. Phys.* **1999**, *153*, 225−272.
(23) Fabiano, E.; Keal, T. W.; Thiel, W. Implementation of Surface Hopping Molecular Dynamics Using Semiempirical Methods. *Chem. Phys.* **2008**, *349*, 334−347.
(24) Qiu, J.; Bai, X.; Wang, L. Crossing Classified and Corrected Fewest Switches Surface Hopping. *J. Phys. Chem. Lett.* **2018**, *9*, 4319−4325.
(25) Wang, L.; Beljonne, D. Flexible Surface Hopping Approach to Model the Crossover from Hopping to Band-like Transport in Organic Crystals. *J. Phys. Chem. Lett.* **2013**, *4*, 1888−1894.
(26) Wang, L.; Prezhdo, O. V. A Simple Solution to the Trivial Crossing Problem in Surface Hopping. *J. Phys. Chem. Lett.* **2014**, *5*, 713−719.
(27) Ryabinkin, I. G.; Nagesh, J.; Izmaylov, A. F. Fast Numerical Evaluation of Time-Derivative Nonadiabatic Couplings for Mixed Quantum−Classical Methods. *J. Phys. Chem. Lett.* **2015**, *6*, 4200−4203.
(28) Fernandez-Alberti, S.; Roitberg, A. E.; Nelson, T.; Tretiak, S. Identification of Unavoided Crossings in Nonadiabatic Photoexcited Dynamics Involving Multiple Electronic States in Polyatomic Conjugated Molecules. *J. Chem. Phys.* **2012**, *137*, 014512.
(29) Cui, G.; Yang, W. Conical Intersections in Solution: Formulation, Algorithm, and Implementation with Combined Quantum Mechanics/Molecular Mechanics Method. *J. Chem. Phys.* **2011**, *134*, 204115.
(30) Curchod, B. F. E.; Agostini, F. On the Dynamics through a Conical Intersection. *J. Phys. Chem. Lett.* **2017**, *8*, 831−837.
(31) Proppe, A. H.; Elkins, M. H.; Voznyy, O.; Pensack, R. D.; Zapata, F.; Besteiro, L. V.; Quan, L. N.; Quintero-Bermudez, R.; Todorovic, P.; Kelley, S. O.; Govorov, A. O.; Gray, S. K.; Infante, I.; Sargent, E. H.; Scholes, G. D. Spectrally Resolved Ultrafast Exciton Transfer in Mixed Perovskite Quantum Wells. *J. Phys. Chem. Lett.* **2019**, *10*, 419−426.
(32) Oberhofer, H.; Reuter, K.; Blumberger, J. Charge Transport in Molecular Materials: An Assessment of Computational Methods. *Chem. Rev.* **2017**, *117*, 10319−10357.
(33) Nelson, T.; Fernandez-Alberti, S.; Roitberg, A. E.; Tretiak, S. Artifacts Due to Trivial Unavoided Crossings in the Modeling of Photoinduced Energy Transfer Dynamics in Extended Conjugated Molecules. *Chem. Phys. Lett.* **2013**, *590*, 208−213.
(34) Nelson, T.; Fernandez-Alberti, S.; Roitberg, A. E.; Tretiak, S. Electronic Delocalization, Vibrational Dynamics, and Energy Transfer in Organic Chromophores. *J. Phys. Chem. Lett.* **2017**, *8*, 3020−3031.
(35) Pradhan, E.; Sato, K.; Akimov, A. V. Non-Adiabatic Molecular Dynamics with ΔSCF Excited States. *J. Phys.: Condens. Matter* **2018**, *30*, 484002.
(36) Cui, G.; Ai, Y.; Fang, W. Conical Intersection Is Responsible for the Fluorescence Disappearance below 365 Nm in Cyclopropanone. *J. Phys. Chem. A* **2010**, *114*, 730−734.
(37) Qiu, J.; Bai, X.; Wang, L. Subspace Surface Hopping with Size-Independent Dynamics. *J. Phys. Chem. Lett.* **2019**, *10*, 637−644.

(38) Akimov, A. V. Libra: An Open-Source "Methodology Discovery" Library for Quantum and Classical Dynamics Simulations. *J. Comput. Chem.* **2016**, *37*, 1626−1649.
(39) Kosloff, D.; Kosloff, R. A. Fourier Method Solution for the Time Dependent Schrödinger Equation as a Tool in Molecular Dynamics. *J. Comput. Phys.* **1983**, *52*, 35−53.
(40) Wang, L.; Trivedi, D.; Prezhdo, O. V. Global Flux Surface Hopping Approach for Mixed Quantum-Classical Dynamics. *J. Chem. Theory Comput.* **2014**, *10*, 3598−3605.
(41) Sato, K.; Pradhan, E.; Asahi, R.; Akimov, A. V. Charge Transfer Dynamics at the Boron Subphthalocyanine Chloride/C_{60} Interface: Non-Adiabatic Dynamics Study with Libra-X. *Phys. Chem. Chem. Phys.* **2018**, *20*, 25275−25294.
(42) Akimov, A. V.; Smith, B.; Shakiba, M.; Sato, K.; Temen, S.; Li, W.; Sun, X.; Chan, M. *Quantum-Dynamics-Hub/Libra-Code: Hotfix for the TD-DFT/NAMD with Libra*, ver. 4.9.1; Zenodo: 2020.

NOTE ADDED AFTER ASAP PUBLICATION

Due to an ACS production error, this paper was originally published ASAP with incorrect pagination. This was corrected in the version published on January 14, 2021.

https://dx.doi.org/10.1021/acs.jpclett.0c03428
J. Phys. Chem. Lett. 2021, 12, 850−860